Human Molecular Genetics, 2017, Vol. 26, No. 8 1432–1443

doi: 10.1093/hmg/ddx042
Advance Access Publication Date: 31 January 2017
Original Article

ORIGINAL ARTICLE

ATPase-deficient mitochondrial inner membrane protein ATAD3A disturbs mitochondrial dynamics in dominant hereditary spastic paraplegia

Helen M. Cooper[1,†], Yang Yang[2,3,†], Emil Ylikallio[2,4], Rafil Khairullin[5,6], Rosa Woldegebriel[2], Kai-Lan Lin[1], Liliya Euro[2], Eino Palin[2], Alexander Wolf[7], Ras Trokovic[2], Pirjo Isohanni[2,8], Seppo Kaakkola[4], Mari Auranen[2,4], Tuula Lönnqvist[8], Sjoerd Wanrooij[5] and Henna Tyynismaa[2,9,*]

[1]Åbo Akademi University, Faculty of Natural Sciences and Technology, Turku, Finland, [2]Research Programs Unit, Molecular Neurology, University of Helsinki, Helsinki, Finland, [3]Institute of Neuroscience, Zhejiang University School of Medicine, Hangzhou, P.R. China, [4]Clinical Neurosciences, Neurology, University of Helsinki and Helsinki University Hospital, Helsinki, Finland, [5]Department of Medical Biochemistry and Biophysics, Umeå University, Umeå, Sweden, [6]Institute of Fundamental Medicine and Biology, Kazan (Volga Region) Federal University, Kazan, Russia, [7]Institute of Molecular Toxicology and Pharmacology, Helmholtz-Zentrum Muenchen-German Research Center for Environmental Health, Neuherberg, Germany, [8]Department of Child Neurology, Children's Hospital, Helsinki University Hospital, Helsinki, Finland and [9]Department of Medical and Clinical Genetics, University of Helsinki, Helsinki, Finland

*To whom correspondence should be addressed at: Biomedicum Helsinki, r.C520b, Haartmaninkatu 8, 00290 Helsinki, Finland. Tel: +358 5044 86394; Fax: +358 2941 25610; Email: henna.tyynismaa@helsinki.fi

Abstract

De novo mutations in *ATAD3A* (ATPase family AAA-domain containing protein 3A) were recently found to cause a neurological syndrome with developmental delay, hypotonia, spasticity, optic atrophy, axonal neuropathy, and hypertrophic cardiomyopathy. Using whole-exome sequencing, we identified a dominantly inherited heterozygous variant c.1064G > A (p.G355D) in *ATAD3A* in a mother presenting with hereditary spastic paraplegia (HSP) and axonal neuropathy and her son with dyskinetic cerebral palsy, both with disease onset in childhood. HSP is a clinically and genetically heterogeneous disorder of the upper motor neurons. Symptoms beginning in early childhood may resemble spastic cerebral palsy. The function of ATAD3A, a mitochondrial inner membrane AAA ATPase, is yet undefined. AAA ATPases form hexameric rings, which are catalytically dependent on the co-operation of the subunits. The dominant-negative patient mutation affects the Walker A motif, which is responsible for ATP binding in the AAA module of ATAD3A, and we show that the recombinant mutant ATAD3A protein has a markedly reduced ATPase activity. We further show that overexpression of the mutant ATAD3A fragments the mitochondrial network and induces lysosome mass. Similarly, we observed altered dynamics of the mitochondrial

[†]The authors wish it to be known that, in their opinion, the first two authors should be regarded as joint First Authors.
Received: October 20, 2016. **Revised:** January 23, 2017. **Accepted:** January 24, 2017

network and increased lysosomes in patient fibroblasts and neurons derived through differentiation of patient-specific induced pluripotent stem cells. These alterations were verified in patient fibroblasts to associate with upregulated basal autophagy through mTOR inactivation, resembling starvation. Mutations in *ATAD3A* can thus be dominantly inherited and underlie variable neurological phenotypes, including HSP, with intrafamiliar variability. This finding extends the group of mitochondrial inner membrane AAA proteins associated with spasticity.

Introduction

Hereditary spastic paraplegia (HSP) is a disorder of the upper motor neurons leading to spastic weakness of the lower limbs (1). Symptoms can be present at birth, or develop gradually during childhood or adulthood, and intrafamilial clinical variability is often observed (2). Non-complicated HSP presents typically with pyramidal signs and bladder dysfunction, whereas complicated forms may include cerebellar or extrapyramidal signs, epilepsy, cognitive impairment and axonal neuropathy (3). Cerebral palsy (CP) is a non-progressive developmental disorder of the fetal or infant brain that causes problems with movement and posture, and can include spasticity, dyskinesia or ataxia (4). In most cases, CP results from cerebral insults occurring during pregnancy or in the perinatal period, although a substantial genetic contribution has also been proposed (5). Spastic diplegic CP may not be easily distinguishable from HSP particularly when family history is negative (6).

The known HSP genes take part in a range of cellular activities such as microtubule dynamics, endoplasmic reticulum morphogenesis, lysosomal and mitochondrial functions and lipid metabolism (1). Of the mitochondria-mediated HSP, *SPG7* is the best studied disease gene (7). It encodes paraplegin, a subunit of an AAA (ATPase associated with diverse cellular activities) protease of the inner mitochondrial membrane. AAA proteins typically form hexameric ring complexes that are catalytically active only in the fully assembled state, and show cooperativity among the six subunits (8). Paraplegin forms hetero-oligomers with another mitochondrial AAA protein AFG3L2, which is associated with early-onset spasticity with ataxia (9).

A recurrent *de novo* mutation in *ATAD3A* (ATPase family AAA-domain containing protein 3A) leading to the amino acid change p.R528W was recently described in patients with global developmental delay, hypotonia, spasticity, optic atrophy, axonal neuropathy, and hypertrophic cardiomyopathy (10). ATAD3A is a nuclear-encoded mitochondrial inner membrane ATPase with functions implicated in the control of mitochondrial dynamics (11), cholesterol channeling (12), and the maintenance of the mitochondrial DNA-protein complexes, the nucleoids (13–15). ATAD3A is anchored to the mitochondrial inner membrane with the N-terminus having contact sites with the outer membrane (11). Its C-terminal AAA ATPase domain is located in the mitochondrial matrix and contains the conserved Walker A and B motifs for ATP binding and ATPase activity, respectively (16,17). Expression of a Walker A mutant incapable of ATP binding resulted in fragmentation of the mitochondrial network in a glioblastoma cell line (11). Expression of the Drosophila mutant equivalent to the human *de novo* mutation R528W affected survival in flies, except when driven only to the muscles, where it resulted in a reduction in the number of mitochondria, presenting with small size and aberrant cristae, and in increased amounts of autophagic intermediates (10). Induction of mitophagy, the autophagy of mitochondria, was also reported in a R528W patient's fibroblasts, based on transmission electron microscopy (10). The authors concluded that the *de novo* mutation was likely to have a strong dominant-negative effect.

We report here dominant transmission of an ATPase-deficient Walker A mutation in *ATAD3A*, presenting as hereditary spastic paraplegia and tetraplegia within the same family.

Results

Clinical description

Patient II:1 is a 35-year-old female with congenital lower leg spasticity (Fig. 1A and C). She was born to healthy parents of a normal pregnancy, and without perinatal problems. The patient's father died at the age of 45 of an unknown cause, following excessive alcohol consumption. The family has origins in Northern Finland, Moldova and Russia.

The patient learned to speak and was able to stand with support around one year of age, and started to walk short distances at the age of three years. Because of her lower leg spasticity, both her Achilles tendons have been operated at an early age. Since childhood the patient has had strong myopia with a level of minus 10 diopters. She had no learning difficulties at school, and performed well academically. In adulthood, the spasticity has remained relatively stable. The patient has been otherwise healthy, apart from a goiter that was operated at the age of 33.

Patient II:1's brain MRI was normal. Her spinal cord seemed thin and atrophic, without any focal signs or signals (Fig. 1B). An electroneuromyography (ENMG) showed moderate chronic motor and sensory axonal neuropathy. A blood test showed the patient's thyroid function to be normal, her creatine kinase was 100 IU/l (reference range 35–210 IU/l), and lactate 0.7 mmol/l (reference range 0.5–2.2 mmol/l). Blood pyruvate was slightly increased at 71 μmol/l (reference range 40–70 μmol/l). A cardiac examination performed at the age of 18 was normal.

In a neurological examination at the age of 35 the patient was found to be 158 cm tall with a BMI of 18. She walked with two sticks aided by one person. She had no problems in speech, cognition, or eye movements. No ptosis was noted but she had significant photophobia that restricted eye opening. The muscle strength and tone of her upper limbs were normal. In her lower limbs, she had strong spasticity and deformity in her knees and ankles (Fig. 1A). Muscle strength in her lower limbs was clearly reduced especially distally, but overcame gravity. Tendon reflexes were lost at the ankles, but found at the knee level and in the arms. Sensory testing was normal apart from abnormal proprioception in the lower legs. Babinski and Hoffman signs were positive.

The patient's only child (III:1, Fig. 1C) is a 3.5-year-old male. He was born at gestational week 39 by cesarean section because of his mother's condition. His Apgar scores were 8/9 and birth weight 3310g. He had no perinatal problems.

The son was sent to hospital at the age of 4 months due to spasticity in his lower extremities. His plasma creatine kinase value was 180 U/l (reference range 50–270 U/l), alanine aminotransferase 20 U/l (reference range < 40 U/l), ammonia 57 μmol/l (reference range < 50 μmol/l) and lactate 2.6 mmol/l (reference range 0.5–2.2 mmol/l). An EEG was performed at the age of 9 months and a brain and cervical spine MRI at the age of 12 months with normal

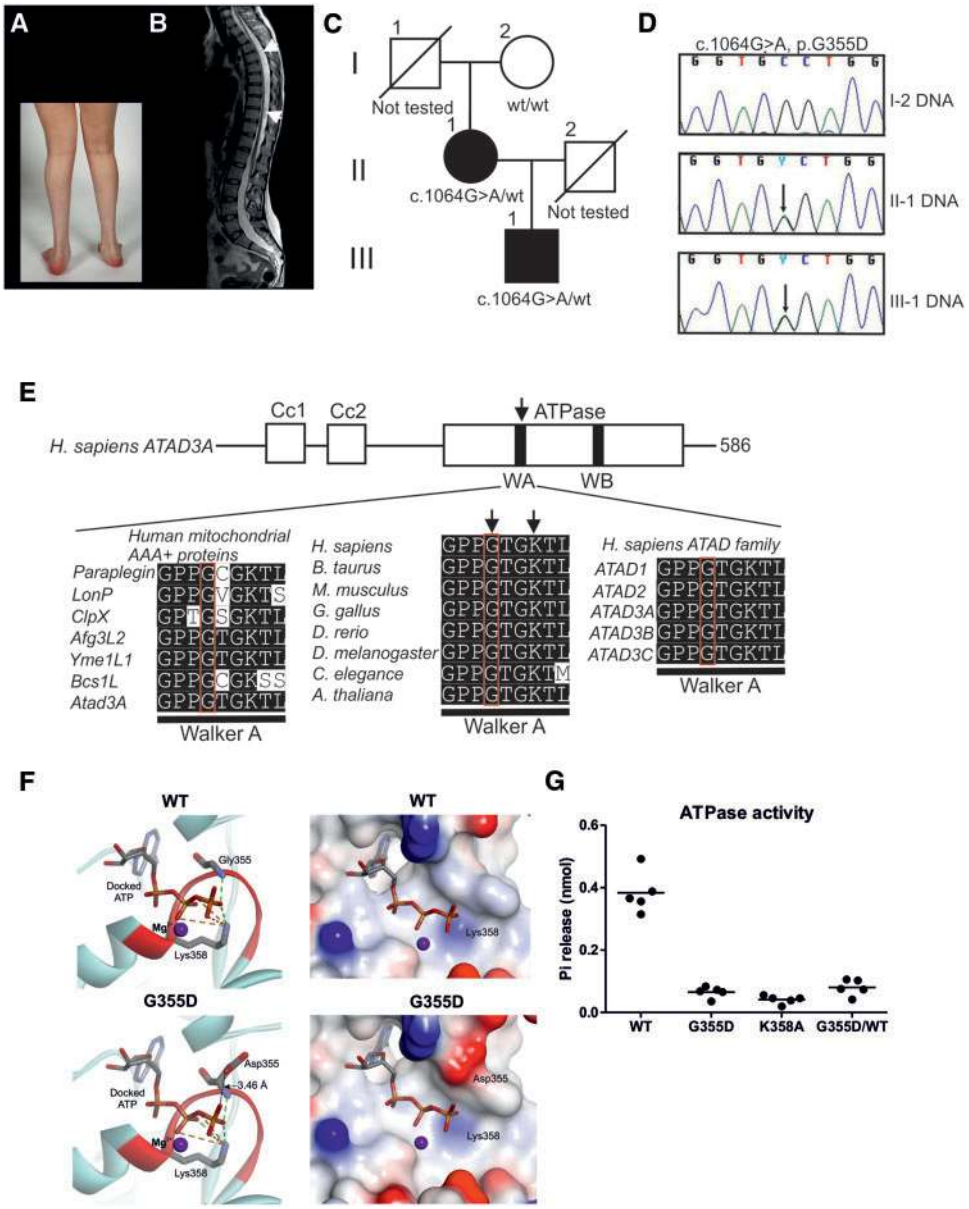

Figure 1. Family with ATAD3A Walker A mutation. (**A**) Patient II-1 (35-year-old, female) has deformity in the lower extremities. (**B**) Magnetic resonance imaging of patient II-1 shows thinning and atrophy of the spinal cord (arrows). (**C**) Pedigree of the investigated family. Grandparents (I:1 and I:2) were not affected. Patient II:1 and her son III:1 have the heterozygous c.1064G > A variant in *ATAD3A*. (**D**) Sanger sequencing of the *ATAD3A* c.1064G > A variant in the samples of the family members I:2, II:1 and III:1. (**E**) Schematic presentation of the human ATAD3A protein and conservation of the Walker A motif. ATAD3 proteins contain two coiled-coil domains (Cc1 and Cc2), and an ATPase domain with Walker A (WA) and Walker B (WB) motifs. The glycine in the Walker A motif affected by the patient mutation G355D (arrow) is invariant in ATAD3 proteins between species, in human mitochondrial proteins with AAA modules and in the human ATAD family. The invariant lysine K358 is also indicated by an arrow. (**F**) *In silico* modeling of the G355D mutation suggests that the substitution of glycine 355 to aspartate changes the affinity of the substrate-binding site for ATP. Walker A motif is shown in red. (**G**) ATPase activities of the recombinant ATAD3A proteins (WT, patient mutant G355D and Walker dead K358A) assessed by the amount of phosphate liberated as described in the materials and methods. The measurements of five independent experiments are shown, the mean is indicated. The reactions were performed in the presence of 8 nM of ATAD3A protein. In the combined reactions of wild type and G355D mutant proteins 8 nM of each ATAD3A variant was used.

results. At the age of 3.5 years the patient had dyskinetic cerebral palsy with severe spasticity both in his upper and lower extremities. He was not able to speak, sit or stand, and he could only crawl by pulling himself forwards with his arms or roll on the floor. An ENMG was not performed. His classification in Gross Motor Function Classification System was IV-V and Communication Function System Classification IV-V. Furthermore, he was found to have heavy eyelids giving the impression of ptosis. Similar to his mother, he had lost his lateral eyelashes at about the age of 6 months, and he had photophobia.

Exome sequencing and verification of the *ATAD3A* variant

To identify the genetic cause of the dominantly inherited condition in this family, we performed whole-exome

sequencing on the DNA samples of the affected mother and son. Filtering for variants in known HSP genes did not reveal potential disease-causing variants. A combined analysis of the two exomes resulted in 12 heterozygous single nucleotide variants of interest (Supplementary Material, Table S1). Of these the variant c.1064G > A [p.G355D] (GenBank: NM_001170535.1; chr1:1459319) in *ATAD3A* caught our attention. It was not present in publicly available databases, and had a Combined Annotation Dependent Depletion (CADD) score of 24.3. We confirmed by Sanger sequencing that the affected mother (II:1) and son (III:1) were heterozygous for the variant, whereas the grandmother (I:2) did not carry the variant (Fig. 1D). The grandfather's (I:1) DNA sample was not available for the study.

The amino acid change from glycine to aspartate affects the Walker A motif of the ATPase (Fig. 1E). This phosphate-binding (P-) loop has a consensus pattern of G-X(4)-GK-[TS] (18), with X denoting any amino acid, and the invariant lysine being crucial for nucleotide-binding and hydrolysis. However, the second glycine of the motif GPPGTGKTL is invariant in all ATAD3 homologues from human to Arabidopsis, as well as in other human mitochondrial AAA proteins (Fig. 1E). A structural *in silico* analysis of the mutant suggested that the G355D change has no effect on protein stability, P-loop fold or interactions between K358 and the β- and γ-phosphates of ATP, which are critical for ATPase activity. However, the mutation introduces a negative charge at a distance of less than 4 Å from the γ-phosphate of an incoming ATP in the substrate-binding site (Fig. 1F), which is predicted to result in decreased affinity for ATP. We expressed and purified C-terminal recombinant ATAD3A proteins containing the mitochondrial matrix-localizing ATPase domain (Supplementary Material, Fig. S1), and measured the ATPase activities of wild type and mutant proteins containing the amino acid changes G355D or K358A (the invariant lysine of the Walker A motif). As predicted, the ATPase activities of the Walker A mutant proteins were markedly reduced in comparison to the wild type recombinant protein (Fig. 1G). Membrane AAA ATPases form hexamers that are catalytically dependent on the co-operation of the subunits. The ATP-binding site in each subunit is located at the interface of the neighboring subunit, and the ATP hydrolysis in one subunit triggers conformational changes in the neighboring subunit leading to a unidirectional cycle of ATP hydrolysis within the hexameric ring. If ATP hydrolysis is blocked in one subunit the entire protein is rendered nonfunctional (19). Similarly to other membrane AAA ATPases, ATAD3A is also proposed to form oligomers (11). We thus measured the ATPase activity of wild type ATAD3A mixed with an equal concentration of G355D, and found, as predicted, that the reduced ATP binding of the mutant ATAD3A had a strong dominant-negative effect on the ATPase function (Fig. 1G).

Overexpressed G355D ATAD3A induces mitochondrial fragmentation

Previously, overexpression of a mutant affecting the critical lysine, K358, in the Walker A motif of ATAD3A was shown to induce fragmentation of the mitochondrial network in cultured U373 glioblastoma cells (11). We therefore tested whether the G355D mutant also induced fragmentation when overexpressed. We expressed the wild type ATAD3A, and the K358R and G355D mutants in primary human fibroblasts, together with mitochondria-targeted green fluorescent protein (mitoGFP), and counted the percentages of transfected cells that displayed fragmented mitochondria (Means ± SEM of four independent counts of fragmented cells 0.45% ± 0.45 (mitoGFP), 19.5% ± 2.09 (WT), 37.0% ± 3.45 (K358R), 32.2 ± 3.23 (G355D), Fig. 2A and C, Supplementary Material, Fig. S2). Control cells with only mitoGFP transfected had normal elongated mitochondria, whereas overexpression of wild type ATAD3A ($P = 0.0013$ compared to mitoGFP) or the mutant forms ($P = 0.0001$ for K358R and $P = 0.0001$ for G355D, compared to mitoGFP) induced mitochondrial fragmentation in a proportion of transfected cells. Both mutants induced fragmentation significantly more frequently than the overexpression of the wild type ATAD3A ($P = 0.003$ for K358R and $P = 0.028$ for G355R, compared to WT, Fig. 2C). As tested by Western blotting, all transfected ATAD3A constructs were expressed at similar levels (Fig. 2B). We also detected increased amounts of lysosomes by LysoTracker staining in the cells containing fragmented mitochondria (Fig. 2D).

Basal autophagy is upregulated in patient fibroblasts

Instead of investigating the overexpression cells further, we focused on the patient's fibroblasts with endogenous expression of the mutant ATAD3A. By using immunocytochemistry of mitochondrial markers and by electron microscopy, we detected increases in elongated, unbranched mitochondria in the patient's cells (Fig. 3A and E). While ATAD3A protein levels were normal in patient cells, we noticed an increase in the ratio of respiratory complex IV and II subunits, and a reduction in the level of the mitochondrial fission protein Drp1 in patient cells compared to controls (Fig. 3B). Also, patient mitochondria were hyperpolarized (Supplementary Material, Figs 3 and 5), which has been shown to be a feature of hyperfused mitochondria (20). In addition, large amounts of lysosomes were seen in patient cells by staining with LysoTracker Green (Fig. 3C), and by electron microscopy (Fig. 3E). Quantification of the Lysotracker signal by flow cytometry confirmed the increase of lysosomes in patient fibroblasts compared to controls (Fig. 3F, Supplementary Material, Fig. S4). We then used Western blotting to inspect markers related to autophagy in patient cells under fed and serum starved conditions and when autophagy was inhibited with bafilomycin (Fig. 3D). The levels of p62, which is degraded during autophagic flux, were found to be constitutively low in patient cells, suggestive of upregulated basal autophagy (21). To investigate the upstream signaling events leading to the lysosomal increase, we assessed the phosphorylation of the autophagy-initiating kinase ULK1 and the ribosomal protein S6, both of which are targets of the autophagy regulator mTOR (22,23). ULK1 was dephosphorylated at Ser757 in patient cells compared to controls under fed and starved conditions (Fig. 3D) (24). This demonstrated that mTOR was inhibited in patient cells, thereby suggesting that AMPK promoted the increase in macroautophagy via ULK1 (24). Levels of total mTOR and phosphorylated mTOR in patient cells were comparable to those in controls. S6 phosphorylation at Ser235/236 was decreased in patient cells compared to controls (Fig. 3D), suggestive of a general downregulation of protein synthesis. The patterns of all of these markers in patient cells in all conditions were remarkably similar to the control cells under starvation, highly suggesting that the mutant cells were in a starvation-like state. The elongation of mitochondria is likely a consequence of the upregulated autophagy, since mitochondrial elongation during autophagy has been shown to spare them from degradation and sustain cell viability (20). Collectively, these data indicate that the

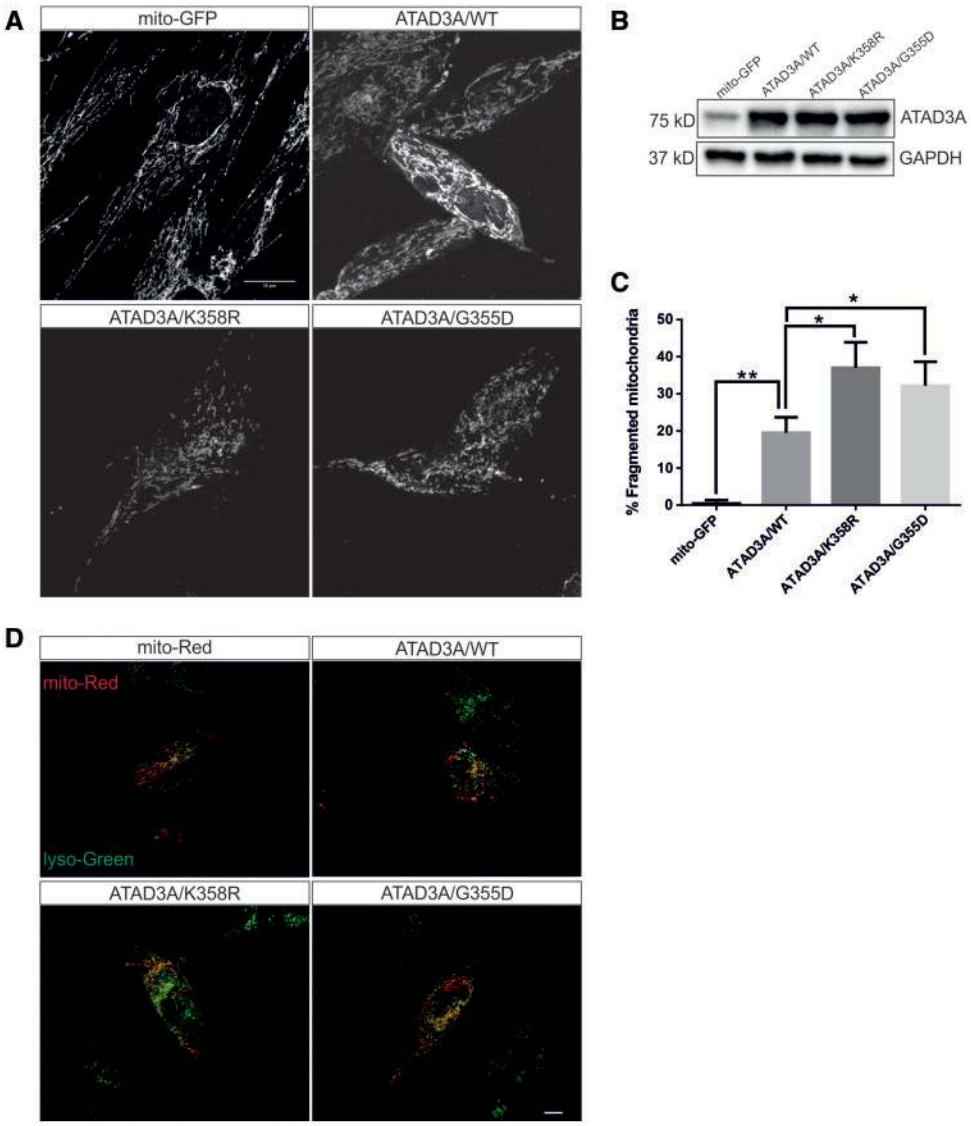

Figure 2. Overexpressed Walker A mutants induce mitochondrial fragmentation. (**A**) Fluorescent microscopy images of primary human fibroblasts transfected with mitochondria-targeted green fluorescent protein (mito-GFP) alone or together with wild type ATAD3A (WT), or ATAD3A Walker A mutants K358R or G355D. ATAD3A immunocytochemistry with ATAD3 antibody is shown. See Supplementary Material, Fig. S2 for merged images. (**B**) Western blotting shows equal levels of ATAD3A in cells transfected with WT, or the K358R or G355D mutant ATAD3A. GAPDH is shown as a loading control. (**C**) Quantification of the transfected cells displaying mitochondrial fragmentation in the experiment shown in A. Fragmented cells were manually counted four independent times in a randomized blinded manner ($n = 157$ transfected cells counted for each genotype). Means ± SEM are shown. *$P < 0.05$, **$P < 0.005$, one-way ANOVA with Bonferroni correction. (**D**) Merged images of fibroblasts transfected with WT, K358R or G355D ATAD3A plasmids, and stained with LysoTracker Green (lyso-Green) for lysosomes and MitoTracker Red (mito-Red) for mitochondria. Cells with fragmented mitochondrial networks show increased staining with LysoTracker Green. Scale bars = 20μm.

mutant ATAD3A induced mitochondrial elongation in patient fibroblasts, which was associated with mTOR inhibition leading to the induction of basal macroautophagy.

Altered mitochondrial network and lysosome content in patient neurons

To study the pathology of the *ATAD3A* mutation in neurons, we reprogrammed patient's fibroblasts into pluripotent stem cells and differentiated those into neurons (25) (Supplementary Material, Fig. S6). The differentiation process of the patient cells was similar compared with the controls, and morphologically patient neurons appeared indistinguishable from controls. The neuronal cultures were composed of a heterogeneous cell population, of which approximately 30%–40% stained positive for a neuronal marker TUJ1. Confocal microscopic analysis of neurons immunostained for ATAD3A showed an altered appearance of the mitochondrial network in patient neurons compared to controls (Fig. 4A). In particular, more uniform staining was detected in the extensions of patient neurons, which may indicate elongated mitochondria. On the other hand, electron microscopy also revealed fragmented mitochondria (Fig. 4D, Supplementary Material, Fig. S7), and perinuclear accumulations of mitochondria were observed by confocal microscopy (Fig. 4A). These findings suggested that patient neurons had unbalanced dynamics of mitochondria. Lysotracker staining and electron microscopy showed an increase in

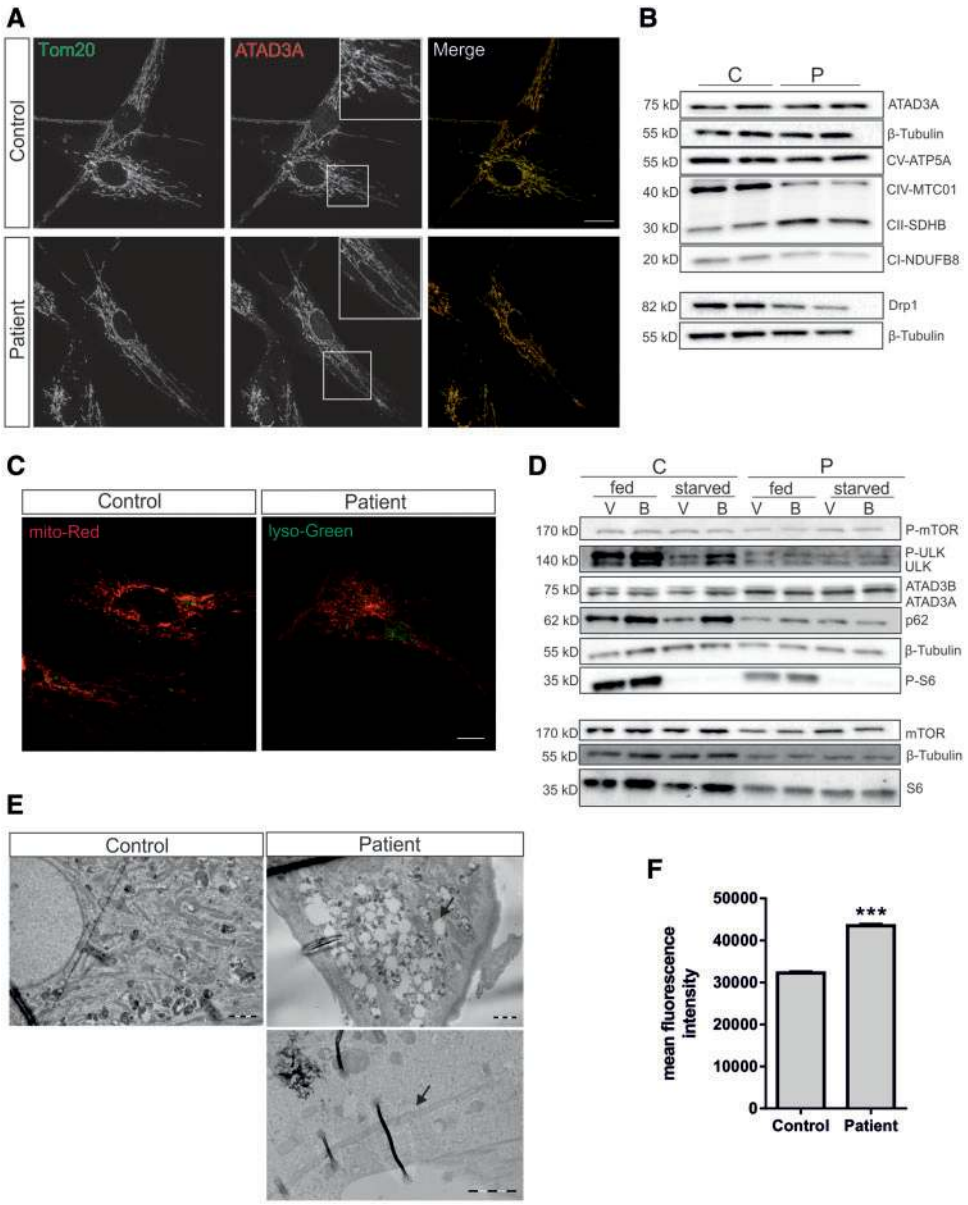

Figure 3. Mitochondrial elongation and upregulation of autophagy in patient fibroblasts. **(A)** Primary patient skin fibroblasts show an elongated mitochondrial morphology when compared with control cells. Mitochondria were immunolabeled with Tom20 (green) and ATAD3A (red) antibodies. **(B)** ATAD3A protein level is unchanged in patient (P) cells, but levels of Drp1 are reduced and the relative amounts of respiratory chain complex subunits are altered compared to controls (C) cells. **(C)** Live cell imaging shows an increase in the number of lysosomes (lyso-Green) and mitochondrial elongation (mito-Red) in patient neurons. Scale bars = 20μm. (D) Phosphorylation and levels of mTOR mediated basal autophagy markers ULK1 (Ser757) and S6 (Ser235/236) are altered in patient (P) cells compared to controls (C) under fed and starved conditions and when autophagy is inhibited (V, vehicle; B, bafilomycin) **(E)** Electron micrographs show large amounts of lysosomal structures (black arrow, upper panel) and unbranched elongated mitochondria (black arrow, lower panel) in the patient fibroblasts. **(F)** Lysosomal quantification by flow cytometry, ($N_{control}$ =24459, $N_{patient}$ = 19517) ***$P < 0.0001$, Student's *t*-test.

lysosomes in patient neurons compared with controls (Fig. 4B, Supplementary Material, Fig. S6). No changes in ATAD3A protein level (Fig. 4C) or mtDNA copy number (Fig. 4E), nor mtDNA deletions (not shown) were observed in samples taken from the mixed neuronal cultures.

Discussion

Our report extends the phenotypes caused by *ATAD3A* mutations to early-onset HSP, and dyskinetic CP, and shows that disease-causing *ATAD3A* mutations can be dominantly inherited. *ATAD3A* should be thus considered a candidate gene in sporadic or dominant HSP. We could not confirm whether the *ATAD3A* mutation was *de novo* in our patient II:1 as her father's DNA sample was not available for study. The phenotypes described recently in patients with the *de novo* R528W mutation have some overlap with our patients, as spasticity and peripheral neuropathy were reported in four of five patients (10). However, neither of our patients had optic atrophy or hypertrophic cardiomyopathy, and our patient II:1 did not have developmental delay or intellectual disability. A diagnostic clue may be provided by photophobia, which both of our patients had.

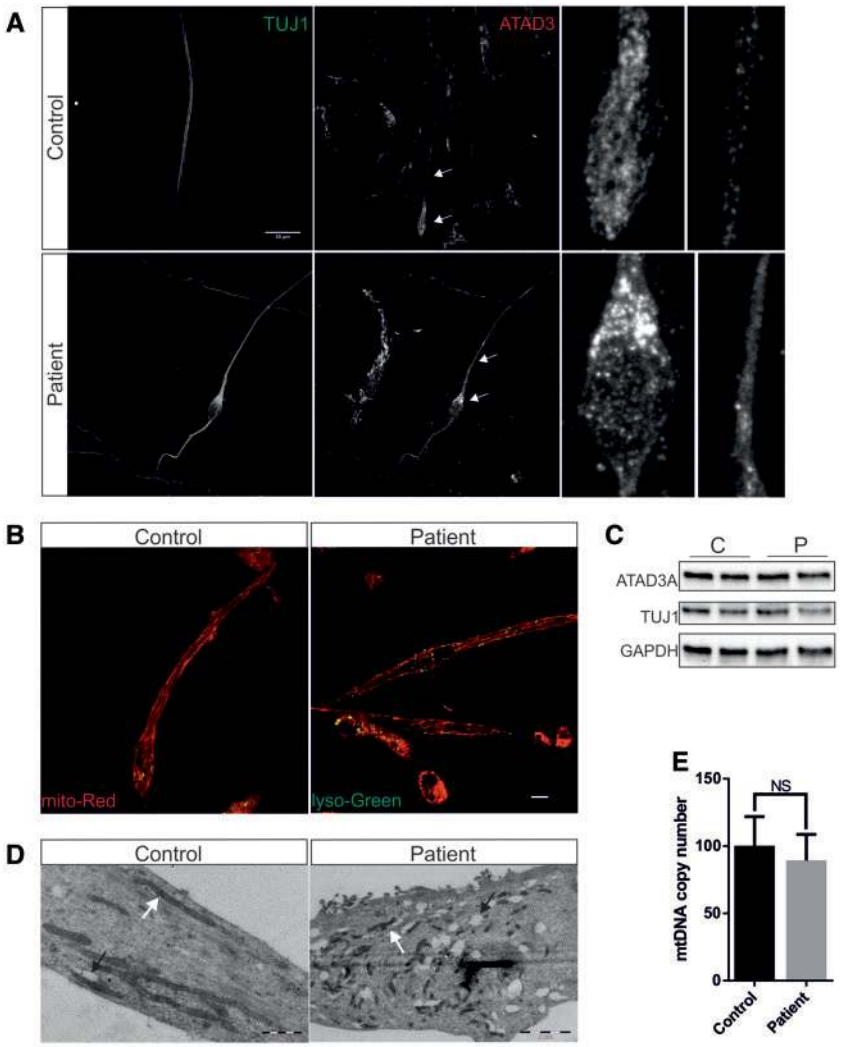

Figure 4. Increased lysosomes in patient-specific neurons. (**A**) Neurons derived through differentiation of ATAD3A patient's induced pluripotent stem cells show altered appearance of the mitochondrial network and ATAD3 immunostaining compared to control neurons. Neurons were identified with TUJ1 (green), and labelled with ATAD3 antibody (red). The white arrows point to the neuronal soma and an extension, which are enlarged on the right. (**B**) Increased lysosomal structures are seen in patient neurons as stained with Lysotracker Green. (**C**) Patient (P) neuronal cultures have a comparable ATAD3A protein level to control (C) cells. (**D**) Electron micrographs show large amounts of lysosomal structures (black arrow) in the patient neurons. White arrows point to mitochondria. (**E**) The mitochondrial DNA copy number was comparable to control cells in the patient neuronal culture, as determined by quantitative PCR. NS, non-significant, Student's *t*-test.

Our family also demonstrates intrafamilial phenotypic variability, which is often seen in association with HSP (2).

We showed that the patient mutation, changing glycine to aspartate in the ATP-binding Walker A motif, markedly reduced the ATPase activity of ATAD3A *in vitro*, but did not affect the steady-state amount of the ATAD3A protein in patient cells. Furthermore, we showed that the mutant protein mixed with the wild type protein abolished the activity of the wild type enzyme. Thus the molecular defect in our patients is directly related to the loss of ATPase activity, which is mediated by a dominant-negative effect on the oligomeric protein (11). Other mitochondrial AAA proteins such as paraplegin function as hexameric rings (26). Their chaperone-like and proteolytic activities have important roles in mitochondrial protein quality control, but in addition to the AAA module, they also have a conserved proteolytic domain that is not present in ATAD3A. Mammalian ATAD1, which also lacks the proteolytic domain, has recently been assigned a role in the mitochondrial protein quality control system, where it mediates the degradation of tail-anchored ER proteins that have been mislocalized to mitochondria (27). The mitochondrial target of the ATPase activity of ATAD3A is, however, still not known.

Human ATAD3, which refers to the two mitochondrial paralogs, ATAD3A and ATAD3B, has been implicated in the maintenance of mitochondrial nucleoids and their membrane attachment (13–15). In our patient neurons with the ATAD3A defect, we did not observe changes in the quality or quantity of mitochondrial DNA. It is not yet clear what contribution each ATAD3 paralog has in cells and different tissue types. One study found ATAD3B to function as dominant negative for the ubiquitous ATAD3A (28), whereas ATAD3B has been found highly expressed in cells with proliferative potential, and frequently in

cancer cells (29). Mice only have one Atad3 gene, and its knockout is embryonic lethal (30).

ATAD3 has been suggested to locate to contact points of the outer and inner mitochondrial membranes (23), and to be enriched in mitochondria associated membranes (MAM) (12,13), implying contact with the endoplasmic reticulum (29). The ER contacts are important for transit of newly made proteins, lipids and calcium. As a genetically heterogeneous disease, HSP is associated with several cellular pathways, such as abnormalities in axonal transport, ER morphology, mitochondrial function, protein misfolding leading to ER stress, vesicle formation and membrane trafficking, and lipid metabolism (31). The mechanism of ATAD3A in neurological diseases could be linked to several of these pathways. It is, however, interesting that paraplegin, AFG3L2 and HSP60, all important for mitochondrial protein homeostasis, have also been connected to spasticity phenotypes (7,9,32). This could imply that ATAD3A may function in mitochondrial protein quality control perhaps through a similar mechanism as ATAD1. On the other hand, paraplegin also contributes to the assembly of the mitochondrial ribosome (33), and ATAD3 has been reported to bind the mitoribosome and to be required for mitochondrial protein synthesis (15). Our observation that the ratio of respiratory chain complex IV and II subunits was increased in patient fibroblasts suggests a defect related to mitochondrial gene expression, typically seen as a reduction in complex IV and a compensatory increase in complex II, which in contrast to the other complexes does not contain mtDNA-encoded subunits. ATAD3 is also needed for maintaining cristae structure (13), the loss of which will compromise the respiratory chain. Therefore, there are multiple possibilities for how ATAD3A dysfunction could cause HSP.

In our patient's fibroblasts, the reduced ATPase activity of ATAD3A was associated with changes in mitochondrial morphology, in particular as highly elongated mitochondria. In patient neurons elongated mitochondria were also observed as well as perinuclear accumulations of mitochondria. These results suggested that the dynamics of mitochondria was altered. ATAD3 knockdown has previously been found to result in aberrant mitochondrial morphology, most notably a collapse of mitochondrial membrane structure (13). Our overexpression experiments in primary fibroblasts indicated that the high-level expression of ATPase deficient mutants and also the wild type ATAD3A caused mitochondrial fragmentation. Collectively, these results suggest that a proper amount of functional ATAD3A is needed to keep the mitochondrial dynamics in balance.

We found the altered mitochondrial dynamics to be associated with greatly increased lysosome mass in overexpression cells, patient fibroblasts and neurons. Previously, the electron micrographs of fibroblasts from a patient with the *de novo* R528W mutation were reported to show increased mitophagic vesicles (10), and ATAD3 knockdown to induce autophagy (34). We studied the patient fibroblasts in more detail for autophagy induction, and found the markers to indicate the induction of basal autophagy in these cells. In particular the combination of low levels of p62, the dephosphorylated ULK1-Ser757 and the reduced phosphorylation of S6, indicated inactivity of mTOR, resulting in a phenotype resembling cells undergoing starvation. Interestingly, mitochondria are known to elongate in response to starvation-induced autophagy (20), which is thought to protect them from autophagic degradation because of their enhanced ability to maintain ATP production. In fact, mitochondrial elongation is required to prevent starvation-induced cell death (20). The findings in our patient cells suggest that a similar process has been initiated by the ATAD3A mutation. mTOR is inhibited by oxidative stress (35), and could perhaps induce autophagy in response to reactive oxygen species produced in response to the mutant ATAD3A. Alternatively, due to its location at ER-mitochondria junctions and its resemblance to chaperone proteins, a dysfunctional ATAD3A could induce ER stress which, especially in relation to the unfolded protein response, can trigger mTOR-mediated autophagy (36). ATAD3A appears to have a role as an anti-autophagic factor, but whether it is directly or indirectly involved in the regulation of mitochondrial dynamics and/or autophagy, remains to be studied.

In conclusion, we describe an ATAD3A mutation that is dominantly inherited in a family with HSP. Although further genetic evidence from additional families is needed to verify the association of ATAD3A and dominant HSP, we provide clear evidence for the molecular mechanism of this ATAD3A mutation and describe intracellular consequences of ATPase deficiency of ATAD3A. Further studies of this interesting mitochondrial AAA protein are warranted to understand its role in neurological diseases.

Materials and Methods

Patients and controls

Patient and control samples were taken according to the Declaration of Helsinki, with informed consent. The study was approved by the review board of the Helsinki University Hospital. The skin fibroblasts used in the study were derived from patient II:1.

DNA sequencing

For whole-exome sequencing, the exome targets of the patients' DNA were captured with the Agilent Clinical Research Exome followed by Illumina HiSeq 2500 sequencing. The reads were aligned to the hg19 reference genome, using the Burrows-Wheeler Alignment tool and the variants called with the SAMTOOLS package (37,38). We annotated the variants with the ANNOVAR program and added annotations for predicted deleteriousness (Combined Annotation Dependent Depletion (CADD)), and population frequency of variants (Exome Aggregation Consortium (ExAc)). The variants were filtered by criteria: 1) absent from dbSNP build 138 (https://www.ncbi.nlm.nih.gov/SNP/), 2) absent from the Exome ExAC database of ~60,000 unrelated individuals, 3) absent in an in-house database of 277 exomes, 4) predicted to change the amino acid sequence or splice site, and 5) minimum Combined Annotation Dependent Depletion (CADD) score of 10. The identified variant in *ATAD3A* was Sanger sequenced using the following genomic primers: 5'-GGGATAGATAGGCTGCCCCT-3' and 5'-AGGGGAGA CAGAGCAGATGT-3'.

In silico analysis

To access the structural and functional outcome of the G355D change *in silico*, the AAA domain of ATAD3A was modeled using the homologues AAA domain of the bacterial AAA protease FtsH as a template (PDB id 1lv7). The sequence identity and similarity between AAA domains of these two proteins are 20.8% and 39.4%, respectively. An ATP molecule was docked into the ATP-binding site of the model using the Discovery studio 4.5 software (BIOVIA).

Purification of recombinant ATAD3A protein

A DNA fragment encoding the ATAD3A c-terminus (264AA-568AA) was cloned into the pGEX-6P-2 vector using the BamHI and XhoI restriction sites. This clone was used to generate the ATAD3A G355D and K358R mutant pGEX-6P-2 constructs. Rosetta 2(DE3) *E.coli* cells were transformed with the pGEX-6P-2-ATAD3A expression plasmid. An overnight culture was grown at 37 °C and used to inoculate 3 liters of TB medium. The culture was grown at 37 °C to an OD600 = 0.8, then the temperature was reduced to 18 °C and expression induced with 0.5 mM IPTG for 20 h. Cells were harvested by centrifugation at 5.000 x g for 15 min at 4 °C. Pellets were first washed and then resuspended in ice-cold lysis buffer (25mM HEPES pH 7.4, 200 mM NaCl, 5 mM b-mercaptoethanol, 10% glycerol, protease inhibitors (10 μM AEBSF, 2 μM Bestatin, 1 μM Pepstatin, 2 μM E64) and 0.2 mg/ml DNase. Next, cells were disrupted using the Constant cell disruption system (Constant Systems Ltd). Cell lysates were clarified by centrifugation at 25.000 x g for 60 min and incubated with glutathione sepharose beads for 2.5 h at 4 °C (GE Healthcare). The beads were washed with 50 ml buffer A (25mM HEPES pH 7.4, 200 mM NaCl, 5 mM EDTA, 5 mM b-mercaptoethanol, 5% glycerol, protease inhibitors and 0.05% TritonX100), followed by a 50 ml buffer B wash (25 mM HEPES pH 7.4, 200 mM NaCl, 5 mM b-mercaptoethanol and 5% glycerol), followed by a 10 ml buffer C wash (25mM HEPES pH 7.4, 100 mM KCl, 1 mM ATP, 1 mM $MgCl_2$, 5 mM b-mercaptoethanol, 5% glycerol) and finally by a 10 ml buffer D wash (25mM HEPES pH 7.4, 50 mM NaCl, 5 mM b-mercaptoethanol, 5% glycerol). The GST-ATAD3A fusion protein was eluted with buffer D supplemented with 40 mM reduced glutathione. GST-ATAD3A-containing fraction were combined and loaded on a 1 ml heparin column (GE Healthcare). After washing the column with buffer D, buffer D containing 1.2M NaCl was used to elute the protein. Fractions containing GST-ATAD3A were combined and incubated with 1:25 weight/weight homemade HIS-tagged HRV 3C protease (Umeå Protein Expertise Platform) in the same buffer overnight. Next day the samples were loaded on a Ni-NTA agarose (Qiagen) to remove the HRV 3C protease. The next day the protein was passed through a PD-10 column (GE Healthcare) and untagged ATAD3A protein was purified on further on a heparin column as described above. Peak fractions were frozen in liquid N2 and stored at −80 °C.

ATPase assay

The ATPase assay was performed in a buffer containing 50 mM Tris-HCl (pH 8.0), 70 mM NaCl/KCl, 2 mM $MgCl_2$, 1 mM ATP and 1 mM DTT in a reaction volume of 50 μl. Reaction mixtures containing 8 nM ATAD3A were incubated for 30 min at 32 °C. 100 μl of BIOMOL Green reagent (Enzo Life Sciences) was added to the reaction followed by a 25 min incubation before measuring the absorbance at 620 nm using an ELISA multiplate reader (Sunrise, Tecan). The amount of phosphate released was calculated using a phosphate standard and used according to the manufacturer's instructions (Enzo Life Sciences).

Overexpression of ATAD3A in primary fibroblasts

Human *ATAD3A* cDNA was cloned into the pcDNA5 vector (Invitrogen) using BamHI and XhoI restriction sites. Primers used for amplification were: 5'-GCCGGATCCGGAATGTC GTGGCTCTTCGGCATT-3', and 5'-CGCCTCGAGTCAGGATGGGGA GGGCTCGTC-3'. Site-directed mutagenesis was conducted to introduce the G355D mutation with primers 5'-ATGTACGGG CCACCAGACACCGGGAAGACG-3', and 5'- CGTCTTCCCGGTGTC TGG TGGCCCGTACAT-3' using the Pfu polymerase (Thermo Fisher). The plasmid sequences were verified by Sanger sequencing. Primary human fibroblasts were cultured in DMEM/FBS/L-Glutamine/Uridine in 37°C, 95% Oxygen, 5% CO_2. Plasmid transfections to the cells were conducted according to the manufacturer's instructions using jetPRIME in vitro DNA & siRNA transfection reagent (Polyplus). Cells for immunocytochemistry were co-transfected with mitochondria-targeted red fluorescent protein (mito-Red) (pDsRed2-Mito Vector, Clontech) or mito-GFP (pAcGFP1-Mito Vector, Clontech).

Cell culture and reprogramming

Primary fibroblasts were reprogrammed using the combination of six factors (OCT3/4, SOX2, KLF4, L-MYC, LIN28 and T53 shRNA) in three episomal plasmids on matrigel coated plates (39). The control line HEL11.4 has been thoroughly characterized previously (40). For the characterisation of the patient's iPSC lines, immunocytochemistry and quantitative PCR were performed (Supplementary Material, Fig. S3). For immunocytochemistry the iPSC were fixed at room temperature with 4% paraformaldehyde for 10 min. Non-specific proteins were blocked by ultra V block (Thermo Fisher). Cells were then treated with primary antibodies overnight at 4°C. Primary antibodies against OCT4 (1:500, SC-9081; Santa Cruz Biotechnology), SSEA4 (1:1000, MC-813-70; Millipore), and TRA-1-60 (1:500, MA1-023; Thermo Fisher) were used to detect stem cell-specific markers. After washing with PBS, cells were incubated with fluorescence-conjugated secondary antibody Alexa Fluor 488: donkey anti-rabbit (1:500, A21206; Thermo Fisher) and donkey anti mouse (1:500, A21206; Thermo Fisher). The nuclei were mounted with 4',6-diamidino-2-phenylindole (Vectashield; Vector Laboratories). For quantitative PCR total RNA was extracted from iPSC using a NucleoSpin RNA II kit (Macherey-Nagel). DNA was digested in a separate reaction using DNaseI (Promega). Two micrograms of RNA were used for reverse transcription (RT) reaction that was performed using Moloney murine leukemia reverse transcriptase, random hexamers, and oligoT (Promega) according to the manufacturer's instructions. The quantitative PCR reactions were carried out in a Corbette thermal cycler (Qiagen). The relative expression levels of the genes were calculated by calibrating their CT values with that of the housekeeping gene glyceraldehyde-3-phosphate dehydrogenase (GAPDH) and normalized to human embryonic stem cell line H9 (as reference sample). Primer sequences were as follows: OCT3/4 (5'-TTGGGCTCGAGAAGGATGTG-3' and 5'-TCCTCTCG TTGTGCA TAGTCG-3'), SOX2 (5'-GCCCTGCAGTACAACTCCAT-3' and 5'-TGCCCTGCTGCGAGTAGGA-3'), TDGF1 (5'-GAGATGACAG CAT TTGGC-3' and 5'-GGCAGCAGGTTCTGTTTA-3'), NANOG (5'-CTCAGCCTCC AGCAGATGC-3' and 5'-TAGATTTCATTCTCTG GTTCTGG-3'), GAPDH (5'-GGTCATCCATGACAACTTTGG-3' and 5'-TGAGCTTCCCGTTCAGCTC-3'). Episomal vectors were detected by PCR using the following primers: EBNA1 (5'-ATC GTCAAAGCTGCACACAG-3' and 5'-CCCAGGAGTC CCAGT AGTCA-3') and oriP (5'-TTCCACGAGGGTAGTGAACC-3' and 5'-TCGGGGGTGTTAGAGA CAAC-3').

iPSC-derived neuron differentiation

iPSC were cultured in Essential 8 basal medium (# A1516901, Life Technology) with Essential 8 Supplement (50X, #1517101,

Life Technology) on Matrigel (#356231, BD) coated plates. The cells were differentiated into neurons as adherent cultures on Poly-D-lysine and Laminin coated plates using an established differentiation protocol (25). Briefly, the iPSC were detached using 0.5mM EDTA (#15575, Life Technology) in PBS, then cells were transferred to a suspension culture in 6-well plates (Corning® 3471 Costar®) to initiate the neurosphere stage. The medium used for neurospheres contained DMEM/12, Neurobasal media, GlutaMax, B27 supplement (50X), N2 supplement (100X), and bFGF (40 μg/ml). After 4–6 weeks culturing, the neurospheres were cut into monolayer cultures on Poly-D-lysine (A-003-E, Merke Millipore) and Laminin (L2020, Sigma) coated plates. Differentiated neurons were cultured in medium containing DMEM/12, Neurobasal media, GlutaMax, B27 supplement, and N2 supplement for 2 weeks, and neuronal identity was confirmed with immunostaining using neuronal markers MAP-2 and TUJ1.

Immunocytochemistry

The cells for immunocytochemistry were cultured on cover glasses in 6-well plates. 24 h after transfection, the cells were rinsed in PBS three times, fixed with 4% paraformaldehyde for 10 min at RT, rinsed in PBS three times, incubated in 0.2% Triton 100X in PBS for 15 min and rinsed in TBST (0.1% Tween-20 in PBS) three times. Cells were blocked on coverslips for 2 h at RT with 5% BSA/PBST and incubated in primary antibody for 90 min at RT or overnight at +4°C. The following day, cells were washed with PBST three times for 15 min, then incubated in secondary antibody for 1 h at RT. After repeating washing with PBST three times for 15 min, the cells were mounted with Vectashield Mounting Media with DAPI (H-1200, Vector Laboratories).

Lysotracker quantification by flow cytometry

The Lysotracker Green signal was quantified using flow cytometry. Fibroblasts were incubated with 50nM Lysotracker Green (Thermo Fisher Scientific) or vehicle (DMSO) for 30 min at 37 °C in 5% CO_2, rinsed, trypsinised and collected in 1 ml of PBS + 5% FBS and filtered. The signal of ca. 20, 000 cells was counted for each sample with a BD LSRFortessa flow cytometer exciting with a 488nm laser. Background autofluorescence was corrected for by measuring untreated cells.

Measurement by of mitochondrial membrane potential

Mitochondrial membrane potential was determined by quantifying the signal of the fluorescent probe tetramethylrhodamine (TMRM). Fibroblasts were incubated with 200nM TMRM (SigmaAldrich) in DMEM for 20 min at 37 °C in 5% CO_2, rinsed, trypsinised and collected in 0.5 ml of PBS + 5% FBS and filtered. Cell suspensions were kept at 37 °C until each measurement. The signal of ca. 20,000 cells was counted for each sample with a BD LSRFortessa flow cytometer exciting with a 488nm laser. Background autofluorescence was corrected for by measuring untreated cells.

Microscopy and confocal live cell imaging

After immunocytochemistry, cells were imaged with a Zeiss Axio Observer microscope (Zeiss, Germany) with a 63X oil immersion objective and Apotome.2. The excitation/emission wavelengths (nm) used were: blue (DAPI), 350/461; green (GFP), 498/516; and red (DsRed), 558/583 or with a 3i (intelligent imaging innovations) CSU-W1 confocal spinning disk microscope, with a 100X oil immersion objective and an excitation/emission wavelength (nm) of 490/525, green (GFP) and red (Dsred) 555/580 and images were captured with the Slidebook 6 software (Intelligent Imaging Innovations). Cells were incubated with MitoTracker-Red (MitoTracker® Red FM, M22425, Thermo) and Lyso-Tracker-Green (LysoTracker® Green DND-26, L7526, Thermo) for 15 min in the incubator. Live cell microscopy was performed with a Zeiss LSM880 laser confocal microscope with a 63X oil immersion objective for with the following excitation/emission wavelengths (nm): blue (DAPI), 350/461; green (GFP), 498/516; and red (DsRed), 558/583. Images were captured with Zeiss ZEN Pro software (Zeiss, Germany). Alternatively, cells were imaged live with a Leica TCS SP5 confocal microscope with the following excitation/emission wavelengths (nm): green (GFP), 503/553, and red (DsRed), 570/620, and images were captured with *the* Las AF software (Leica). Statistical analyses were done with Microsoft Excel and GraphPad Prism softwares.

Electron microscopy

The cells for electron microscopy were cultured on cover glass in 6-well plates. The cells were washed two times with PBS, then fixed in 2% glutaraldehyde and 2% formaldehyde for 30 min at 4 °C and then left in 2% glutaraldehyde in PBS at RT. Cells were embedded, and blocks were cut into thin sections and stained with OsO_4 according to the standard procedure of the Laboratory of Electron Microscopy, University of Turku, Finland. The grids were imaged with a JEOL JEM-1400 plus transmission electron microscope equipped with an 11 Mpx Olympus Quemesa digital camera.

Starvation and autophagy inhibition

Patient and control fibroblasts were separately kept in either fed condition in normal medium (DMEM with FBS, L-Glutamine and Uridine) or in a starved condition in HBSS (#24020117, Thermo Fisher) for 4 h. The Bafilomycin-inhibitor (Baf, B1793, Sigma) was used as a lysosomal inhibitor (100nM concentration) and DMSO as a vehicle.

Western blotting

Cells were lysed for protein extraction by incubating for 5 min in RIPA buffer (10X, #9806, Cell Signaling) on ice after washing with PBS twice. Cells were then scraped and sonicated briefly, centrifuged for 10 min at 14,000x g in +4°C. Protein concentrations were measured with Bradford or a Nanodrop 2000 instrument. 20–40μg of protein was run into a 10% or 12% polyacrylamide gel (Bio Rad) at 100V for 10 min and then 150V for 50 min. Semi-dry blotting (Thermo Fisher) was conducted transferring the proteins to a PVDF transfer membrane (Merck Millipore) under 36mA for 65 min. Alternatively, proteins were transferred to a nitrocellulose membrane (Amersham™ Protan™, GE Healthcare Life Sciences) by wet blotting under 45 V for 15 min, then 120 V for 45 min. 5% milk/TBST was used for blocking the membrane for 1 h at RT followed by incubation with primary antibodies overnight in +4 °C. On the following day, the membrane was washed with TBST and incubated with secondary antibody for 1 h at RT. After washing with TBST, ECL Prime Detection Reagent (GE Healthcare) or Clarity™ Western ECL

Substrate (BioRad) was used to detect the bands for imaging with a Chemidoc XRS+ Molecular Imager (Bio-Rad).

Antibodies

ATAD3A [1:3 (IF), 1:10 (WB)], ATAD3 [1:2000 (IF), 1:10000 (WB)], p62 (1:5000, Abnova, H00008878-M01 clone 2C11), COXII (1:1000, EPR 3314), GAPDH (1:1000, CST 14C10), LC3B (1:1500, NB600-1384), β-Tubulin (1:1000, CST 2146), TUJ1 (1:1000, # MMS-435P, BioLegend), Tom20 (1:500 ICC; Santa Cruz sc-11415), HRP anti-rabbit (1:10000, Molecular Probes), HRP anti-mouse (1:10000, Molecular Probes), HRP anti-rat (1:10000, Molecular Probes), anti-rabbit 550 (1:1000, Molecular Probes), anti-mouse 488 (1:1000, Molecular Probes), mToR (1:1000, CST 2972), phospho-mTOR (Ser2481) (1:1000, CST 2974), ULK1 (1:1000, CST 8054), phospho-ULK1 (Ser757) (1:1000, CST 6888), S6 ribosomal protein (1:500, CST 2317), phospho-S6 ribosomal protein (Ser235/236) (1:1000, CST 4858), Drp1 (1:1000, Santa Cruz sc-271583), OXPHOS antibody cocktail (1:250, Abcam, ab110413).

Supplementary Material

Supplementary Material is available at *HMG* online.

Acknowledgements

Riitta Lehtinen is thanked for technical assistance and Christopher Carroll, Riikka Martikainen and Eric Dufour for advice and comments. Biomedicum Stem Cell Center (BSCC) is acknowledged for cellular reprogramming, the Institute for Molecular Medicine Finland FIMM, Technology Centre, and University of Helsinki for the exome capture and sequencing, the Laboratory of Electron Microscopy, University of Turku, for sample preparation and the Cell Imaging Core, Turku Centre for Biotechnology, for assistance with the flow cytometry.
H.T., L.E., E.Y. were funded by the Academy of Finland, H.T., H.C. by Sigrid Juselius Foundation, H.T. by University of Helsinki, H.C. by the Finnish Cultural Foundation, E.Y. by the Helsinki University Hospital, and Y.Y. by China Scholarship Council.

Conflict of Interest statement. None declared.

Funding

Academy of Finland, Sigrid Juselius Foundation, University of Helsinki, the Finnish Cultural Foundation, the Helsinki University Hospital, and China Scholarship Council. Funding to pay the Open Access publication charges for this article was provided by the University of Helsinki.

References

1. Tesson, C., Koht, J. and Stevanin, G. (2015) Delving into the complexity of hereditary spastic paraplegias: How unexpected phenotypes and inheritance modes are revolutionizing their nosology. *Hum. Genet.*, **134**, 511–538.
2. McDermott, C., White, K., Bushby, K. and Shaw, P. (2000) Hereditary spastic paraparesis: A review of new developments. *J. Neurol. Neurosurg. Psychiatry*, **69**, 150–160.
3. Harding, A.E. (1983) Classification of the hereditary ataxias and paraplegias. *Lancet*, **1**, 1151–1155.
4. Colver, A., Fairhurst, C. and Pharoah, P.O. (2014) Cerebral palsy. *Lancet*, **383**, 1240–1249.
5. McMichael, G., Bainbridge, M.N., Haan, E., Corbett, M., Gardner, A., Thompson, S., van Bon, B.W., van Eyk, C.L., Broadbent, J., Reynolds, C., *et al.* (2015) Whole-exome sequencing points to considerable genetic heterogeneity of cerebral palsy. *Mol. Psychiatry*, **20**, 176–182.
6. Rainier, S., Sher, C., Reish, O., Thomas, D. and Fink, J.K. (2006) De novo occurrence of novel SPG3A/atlastin mutation presenting as cerebral palsy. *Arch. Neurol.*, **63**, 445–447.
7. Casari, G., De Fusco, M., Ciarmatori, S., Zeviani, M., Mora, M., Fernandez, P., De Michele, G., Filla, A., Cocozza, S., Marconi, R., *et al.* (1998) Spastic paraplegia and OXPHOS impairment caused by mutations in paraplegin, a nuclear-encoded mitochondrial metalloprotease. *Cell*, **93**, 973–983.
8. Le, D.T., Eckert, T. and Woehlke, G. (2013) Computer simulation of assembly and co-operativity of hexameric AAA ATPases. *PLoS One*, **8**, e67815.
9. Pierson, T.M., Adams, D., Bonn, F., Martinelli, P., Cherukuri, P.F., Teer, J.K., Hansen, N.F., Cruz, P., Mullikin For The Nisc Comparative Sequencing Program, J.C., Blakesley, R.W., *et al.* (2011) Whole-exome sequencing identifies homozygous AFG3L2 mutations in a spastic ataxia-neuropathy syndrome linked to mitochondrial m-AAA proteases. *PLoS Genet.*, **7**, e1002325.
10. Harel, T., Yoon, W.H., Garone, C., Gu, S., Coban-Akdemir, Z., Eldomery, M.K., Posey, J.E., Jhangiani, S.N., Rosenfeld, J.A., Cho, M.T., *et al.* (2016) Recurrent de novo and biallelic variation of ATAD3A, encoding a mitochondrial membrane protein, results in distinct neurological syndromes. *Am. J. Hum. Genet.*, **99**, 831–845.
11. Gilquin, B., Taillebourg, E., Cherradi, N., Hubstenberger, A., Gay, O., Merle, N., Assard, N., Fauvarque, M.O., Tomohiro, S., Kuge, O., *et al.* (2010) The AAA+ ATPase ATAD3A controls mitochondrial dynamics at the interface of the inner and outer membranes. *Mol. Cell. Biol.*, **30**, 1984–1996.
12. Issop, L., Fan, J., Lee, S., Rone, M.B., Basu, K., Mui, J. and Papadopoulos, V. (2015) Mitochondria-associated membrane formation in hormone-stimulated leydig cell steroidogenesis: Role of ATAD3. *Endocrinology*, **156**, 334–345.
13. Gerhold, J.M., Cansiz-Arda, S., Lohmus, M., Engberg, O., Reyes, A., van Rennes, H., Sanz, A., Holt, I.J., Cooper, H.M. and Spelbrink, J.N. (2015) Human mitochondrial DNA-protein complexes attach to a cholesterol-rich membrane structure. *Sci. Rep.*, **5**, 15292.
14. He, J., Mao, C.C., Reyes, A., Sembongi, H., Di Re, M., Granycome, C., Clippingdale, A.B., Fearnley, I.M., Harbour, M., Robinson, A.J., *et al.* (2007) The AAA+ protein ATAD3 has displacement loop binding properties and is involved in mitochondrial nucleoid organization. *J. Cell Biol.*, **176**, 141–146.
15. He, J., Cooper, H.M., Reyes, A., Di Re, M., Sembongi, H., Litwin, T.R., Gao, J., Neuman, K.C., Fearnley, I.M., Spinazzola, A., *et al.* (2012) Mitochondrial nucleoid interacting proteins support mitochondrial protein synthesis. *Nucleic Acids Res.*, **40**, 6109–6121.
16. Bogenhagen, D.F., Rousseau, D. and Burke, S. (2008) The layered structure of human mitochondrial DNA nucleoids. *J. Biol. Chem.*, **283**, 3665–3675.
17. Hubstenberger, A., Merle, N., Charton, R., Brandolin, G. and Rousseau, D. (2010) Topological analysis of ATAD3A insertion in purified human mitochondria. *J. Bioenerg. Biomembr.*, **42**, 143–150.
18. Walker, J.E., Saraste, M., Runswick, M.J. and Gay, N.J. (1982) Distantly related sequences in the alpha- and beta-subunits of ATP synthase, myosin, kinases and other ATP-requiring

enzymes and a common nucleotide binding fold. *embo J.*, **1**, 945–951.
19. Sauer, R.T. and Baker, T.A. (2011) AAA+ proteases: ATP-fueled machines of protein destruction. *Annu. Rev. Biochem.*, **80**, 587–612.
20. Gomes, L.C., Di Benedetto, G. and Scorrano, L. (2011) During autophagy mitochondria elongate, are spared from degradation and sustain cell viability. *Nat. Cell Biol.*, **13**, 589–598.
21. Bjorkoy, G., Lamark, T., Brech, A., Outzen, H., Perander, M., Overvatn, A., Stenmark, H. and Johansen, T. (2005) p62/SQSTM1 forms protein aggregates degraded by autophagy and has a protective effect on huntingtin-induced cell death. *J. Cell Biol.*, **171**, 603–614.
22. Gingras, A.C., Raught, B. and Sonenberg, N. (2001) Regulation of translation initiation by FRAP/mTOR. *Genes Dev.*, **15**, 807–826.
23. Jung, C.H., Jun, C.B., Ro, S.H., Kim, Y.M., Otto, N.M., Cao, J., Kundu, M. and Kim, D.H. (2009) ULK-Atg13-FIP200 complexes mediate mTOR signaling to the autophagy machinery. *Mol. Biol. Cell*, **20**, 1992–2003.
24. Kim, J., Kundu, M., Viollet, B. and Guan, K.L. (2011) AMPK and mTOR regulate autophagy through direct phosphorylation of Ulk1. *Nat. Cell Biol.*, **13**, 132–141.
25. Hamalainen, R.H., Manninen, T., Koivumaki, H., Kislin, M., Otonkoski, T. and Suomalainen, A. (2013) Tissue- and cell-type-specific manifestations of heteroplasmic mtDNA 3243A>G mutation in human induced pluripotent stem cell-derived disease model. *Proc. Natl. Acad. Sci. U. S. A*, **110**, E3622–E3630.
26. Rugarli, E.I. and Langer, T. (2012) Mitochondrial quality control: A matter of life and death for neurons. *embo J.*, **31**, 1336–1349.
27. Chen, Y.C., Umanah, G.K., Dephoure, N., Andrabi, S.A., Gygi, S.P., Dawson, T.M., Dawson, V.L. and Rutter, J. (2014) Msp1/ATAD1 maintains mitochondrial function by facilitating the degradation of mislocalized tail-anchored proteins. *embo J.*, **33**, 1548–1564.
28. Merle, N., Feraud, O., Gilquin, B., Hubstenberger, A., Kieffer-Jacquinot, S., Assard, N., Bennaceur-Griscelli, A., Honnorat, J. and Baudier, J. (2012) ATAD3B is a human embryonic stem cell specific mitochondrial protein, re-expressed in cancer cells, that functions as dominant negative for the ubiquitous ATAD3A. *Mitochondrion*, **12**, 441–448.
29. Li, S. and Rousseau, D. (2012) ATAD3, a vital membrane bound mitochondrial ATPase involved in tumor progression. *J. Bioenerg. Biomembr.*, **44**, 189–197.
30. Goller, T., Seibold, U.K., Kremmer, E., Voos, W. and Kolanus, W. (2013) Atad3 function is essential for early post-implantation development in the mouse. *PLoS One*, **8**, e54799.
31. Fink, J.K. (2013) Hereditary spastic paraplegia: Clinico-pathologic features and emerging molecular mechanisms. *Acta Neuropathol.*, **126**, 307–328.
32. Hansen, J.J., Durr, A., Cournu-Rebeix, I., Georgopoulos, C., Ang, D., Nielsen, M.N., Davoine, C.S., Brice, A., Fontaine, B., Gregersen, N., *et al.* (2002) Hereditary spastic paraplegia SPG13 is associated with a mutation in the gene encoding the mitochondrial chaperonin Hsp60. *Am. J. Hum. Genet.*, **70**, 1328–1332.
33. Nolden, M., Ehses, S., Koppen, M., Bernacchia, A., Rugarli, E.I. and Langer, T. (2005) The m-AAA protease defective in hereditary spastic paraplegia controls ribosome assembly in mitochondria. *Cell*, **123**, 277–289.
34. Chen, T.C., Hung, Y.C., Lin, T.Y., Chang, H.W., Chiang, I.P., Chen, Y.Y. and Chow, K.C. (2011) Human papillomavirus infection and expression of ATPase family AAA domain containing 3A, a novel anti-autophagy factor, in uterine cervical cancer. *Int. J. Mol. Med.*, **28**, 689–696.
35. Desai, B.N., Myers, B.R. and Schreiber, S.L. (2002) FKBP12-rapamycin-associated protein associates with mitochondria and senses osmotic stress via mitochondrial dysfunction. *Proc. Natl. Acad. Sci. U. S. A*, **99**, 4319–4324.
36. Whitney, M.L., Jefferson, L.S. and Kimball, S.R. (2009) ATF4 is necessary and sufficient for ER stress-induced upregulation of REDD1 expression. *Biochem. Biophys. Res. Commun.*, **379**, 451–455.
37. Li, H. and Durbin, R. (2009) Fast and accurate short read alignment with burrows-wheeler transform. *Bioinformatics*, **25**, 1754–1760.
38. Li, H., Handsaker, B., Wysoker, A., Fennell, T., Ruan, J., Homer, N., Marth, G., Abecasis, G. and Durbin, R. and 1000 Genome Project Data Processing Subgroup (2009) The sequence alignment/map format and SAMtools. *Bioinformatics*, **25**, 2078–2079.
39. Okita, K., Matsumura, Y., Sato, Y., Okada, A., Morizane, A., Okamoto, S., Hong, H., Nakagawa, M., Tanabe, K., Tezuka, K., *et al.* (2011) A more efficient method to generate integration-free human iPS cells. *Nat. Methods*, **8**, 409–412.
40. Mikkola, M., Toivonen, S., Tamminen, K., Alfthan, K., Tuuri, T., Satomaa, T., Natunen, J., Saarinen, J., Tiittanen, M., Lampinen, M., *et al.* (2013) Lectin from erythrina cristagalli supports undifferentiated growth and differentiation of human pluripotent stem cells. *Stem Cells Dev.*, **22**, 707–716.